JOURNAL OF SOLID STATE CHEMISTRY **124,** 95–103 (1996)
ARTICLE NO. 0212

Flame Generation of Two New Precursors of Vanadyl Pyrophosphate

Philippe F. Miquel,* Elisabeth Bordes,† and Joseph L. Katz*,[1]

*Department of Chemical Engineering, The Johns Hopkins University, Baltimore, Maryland 21218; and †Département de Génie Chimique, Université de Technologie de Compiègne, B.P. 649, 60206 Compiègne Cedex, France

Received December 11, 1995; in revised form March 4, 1996; accepted March 11, 1996

Two new vanadyl pyrophosphate precursors were produced in a single step operation using a counterflow diffusion flame burner. The technique consists of adding a vanadium and a phosphorus halide to the fuel stream of hydrogen–oxygen flames. Particles nucleate and grow in the flame to an average diameter between 5 and 30 nm. Upon exiting the flame, powders are collected on two stainless steel strips and their crystalline structures are analyzed by x-ray diffraction and Fourier-transform infrared spectroscopy. A strong effect of flame temperature on the crystalline structure of the powders produced is observed. When a high temperature flame is used, the powder collected is a mixture of $VOPO_4 \cdot 2H_2O$ and $(VOPO_4)_{1-x}(VOHPO_4)_x \cdot 2.6H_2O$. This mixture forms γ-$VOPO_4$ upon subsequent reheating at 750°C in a oxidizing atmosphere, and transforms into $(VO)_2P_2O_7$ in an oxygen-free atmosphere at 700°C. When a lower temperature flame is used, the powder collected is $(VOPO_4)_{1-x}(VOHPO_4)_x \cdot 2.9H_2O$, which transforms at 750°C into β-$VOPO_4$ in an oxidizing atmosphere and to $(VO)_2P_2O_7$ at 700°C in an oxygen-free atmosphere. Structural differences between the two vanadyl pyrophosphates are observed. These differences are discussed in terms of the ability of $(VO)_2P_2O_7$ to accommodate various disordered and polytypic structures.

INTRODUCTION

Vanadium–phosphorus oxides are the most widely used catalysts for the selective oxidation of *n*-butane to maleic anhydride. In the extensive literature regarding this very complex mixed oxide system, there is general agreement that the most active catalytic phase is mainly composed of vanadyl pyrophosphate, $(VO)_2P_2O_7$ (1, 2). High reactivity of the catalyst is typically obtained when $(VO)_2P_2O_7$ exhibits predominantly its (100) basal plane. However, the exact nature of the active sites is still a matter of ongoing research. Bordes (1) has suggested that these active sites are related to the ability of the (100) plane to accommodate mixed valence V^{4+}–V^{5+} pairs. Volta *et al.* (3, 4) believe that high reactivity is associated with the presence of $VOPO_4$ domain on the (100) plane of $(VO)_2P_2O_7$ crystals. Busca *et al.* (5) observed an increase in catalytic activity in the presence of disorder along the (200) cleavage. They suggest that the disorder is related to defects associated with the two V atoms in edge sharing octahedra of the basal plane. Using *in situ* high-resolution electron microscopy, Gai and Kourtakis (6) recently showed that during the initiation stage of the catalytic reaction, anionic vacancies actually were formed at the O sites connecting corner-sharing phosphate tetrahedra and vanadium octahedra in the (100) plane. They suggested that this leads to the formation of very reactive vanadyl pairs with adjacent oxygen vacancies which could act as active sites.

$(VO)_2P_2O_7$ is usually prepared by dehydration of a well-known precursor phase, the hemihydrate $VOHPO_4 \cdot 0.5H_2O$, in an oxygen free atmosphere. The latter is formed, for example, by reduction of $VOPO_4 \cdot 2H_2O$ with organic alcohols (2, 7, 8). Layered $VOHPO_4 \cdot 0.5H_2O$ exhibiting mainly (001) planes transform topotactically into platelet crystals of $(VO)_2P_2O_7$ exhibiting mainly (100) planes. Other $VOHPO_4 \cdot yH_2O$ phases, namely with y = 1, 2, 3 and 4, have been isolated and characterized (7, 9). Amorós *et al.* showed that all these $VOHPO_4 \cdot yH_2O$ phases transform into $(VO)_2P_2O_7$ when heated at temperatures between 100 and 500°C in an inert atmosphere (9). It is also known that $VOHPO_4 \cdot yH_2O$ phases transform into $VOPO_4$ phases when heated at the same temperatures in the presence of oxygen (7). Finally, $(VO)_2P_2O_7$ and $VOPO_4$ phases interconvert upon reduction and oxidation.

The ''traditional'' precipitation methods used to produce the hemihydrate are tedious, involving many processing steps. Typically there is mixing of the raw materials, followed by stirring for several hours under reflux, then several washings with alcohol, drying, and finally calcination and activation. These lengthy procedures result in long processing times and often generate environmentally troublesome side streams. In earlier papers, we showed that one can produce mixed oxides with well-defined morpholo-

[1] To whom correspondence should be addressed. E-mail: jlk@jhu.edu.

0022-4596/96 $18.00

gies in a single-step operation by *flame synthesis* using a counterflow diffusion flame burner (10–12). Most recently, we applied this new high-temperature synthesis technique to produce vanadium–phosphorus mixed oxide catalysts (13). We obtained nanostructured V–P–O powders by adding a vanadium chloride and a phosphorus chloride precursor to the fuel stream of the counterflow burner. Two crystalline phases were obtained: in a high temperature flame, a mixture of $VOPO_4 \cdot 2H_2O$ with an unknown $VOH_xPO_4 \cdot yH_2O$ phase, and in a low temperature flame, an unknown $VOH_{x'}PO_4 \cdot y'H_2O$ phase. After dehydration of these phases in helium at 750°C, γ-$VOPO_4$ and β-$VOPO_4$, respectively, were obtained. However, the presence of $(VO)_2P_2O_7$ was not detected.

In the present paper, the flame synthesis technique used to produce these nanostructured V–P–O powders is briefly reviewed. The powders obtained are then further analyzed and compared to known crystalline phases of the V–P–O system. They are shown to be mixed valence V^{4+}–V^{5+}–phosphorus oxides. Their reduction in an oxygen-free atmosphere leads to the formation of $(VO)_2P_2O_7$. The crystalline structure of the $(VO)_2P_2O_7$ thus formed is discussed and characterized as polytypes of the platelet structure.

EXPERIMENTAL SETUP AND PROCEDURE

The vanadyl pyrophosphate precursors were produced in a counterflow diffusion flame burner. This new technique for producing mixed oxides in a single step process has been described in detail elsewhere (10, 12, 14). Therefore, the experimental setup and the procedure used for forming and collecting the powders are reviewed here only briefly.

The counterflow diffusion flame burner consists of two vertically opposed tubes of *rectangular* cross-section (see Fig. 1). The oxidizer (O_2 diluted in argon) flows downward from the top tube, while the fuel (H_2 diluted by argon) flows upward from the bottom tube. To ensure uniform and laminar gas flow, each tube is filled with glass beads held in place by perforated plates. Upon ignition of the gases, a flame is visible in the region where the two opposed gas streams collide. The flame thus generated is very flat and uniform in the horizontal plane. The gas flow along the *vertical* direction of the burner (i.e., the Z axis in Fig. 1) can therefore be considered essentially one-dimensional (10). This allows the use of nonintrusive measurement techniques, such as absorption and emission spectroscopy and light scattering, to follow the formation of the oxides in the flames. Extensive use has been made of these measurement techniques to study, *in situ,* the nucleation and growth of vanadium and phosphorus mixed oxides in flames (13, 15). Figure 2A shows the gas flow geometry in the region between the top and the bottom tube, referred to as the burner gap. The dashed line labeled GSP indicates the location of the gas stagnation plane, which is the hori-

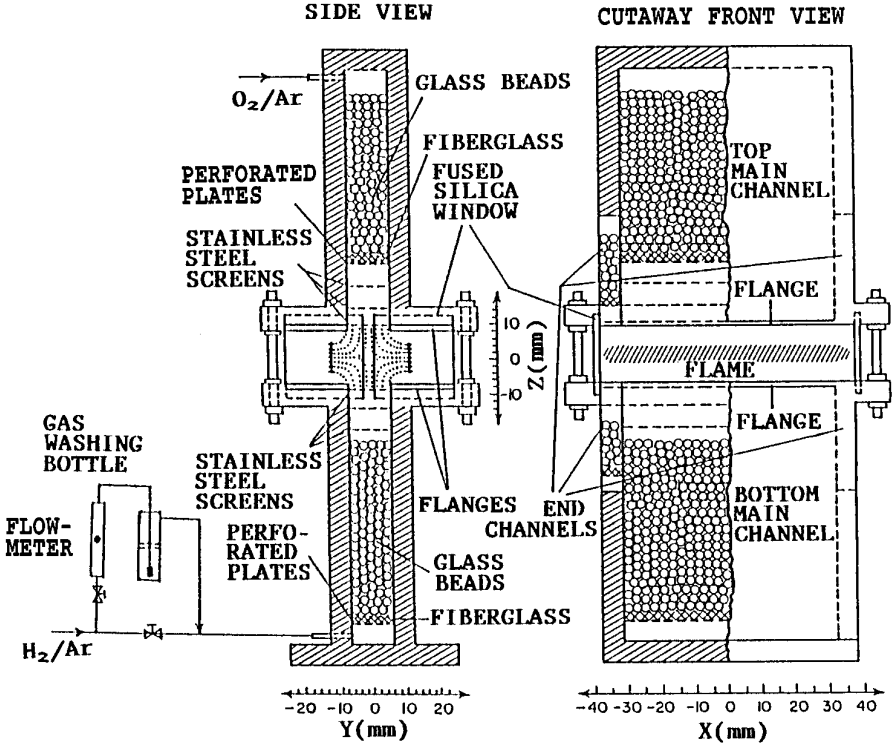

FIG. 1. Front and side view of the counterflow diffusion flame burner.

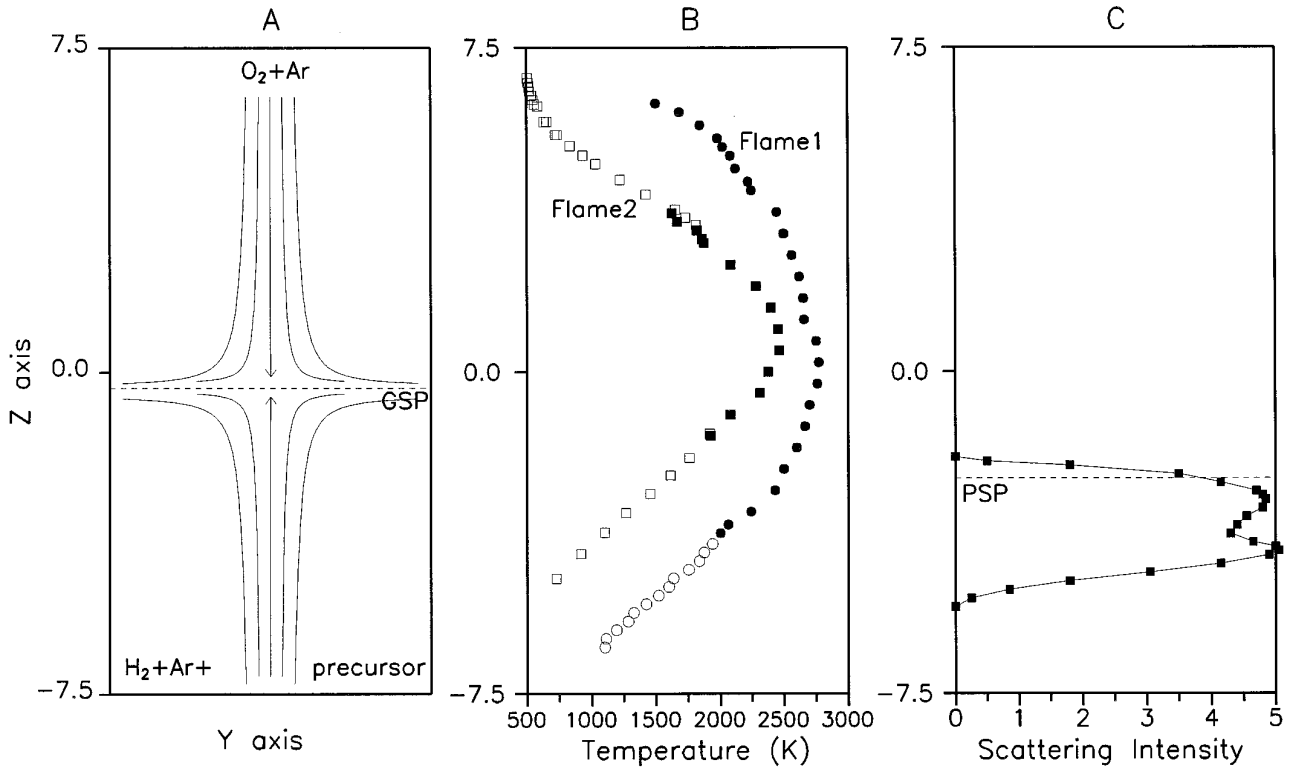

FIG. 2. (A) Gas flow geometry of the hydrogen–oxygen flames; (B) Temperature profiles for Flame 1 and Flame 2; (C) Scattering intensity profile when a 1:1 mixture of PCl_3 and VCl_4 is added to the fuel stream of Flame 2. GSP indicates the location of the gas stagnation plane; PSP indicates the location of the particle stagnation plane.

zontal plane where the two gas streams impinge and flow out of the burner. Figure 2B shows the temperature distributions obtained when using two different sets of gas flow rates (these flow rates are given in Table 1); for convenience these flow rates and the resulting temperature and gas velocity distributions will be referred to as Flame 1 and Flame 2. Temperatures were measured by OH absorption spectroscopy (filled symbols) and by thermocouple (open symbol) as described previously (10, 13).

Mixed vanadium–phosphorus oxides are produced by bubbling a small fraction of the fuel stream through two gas washing bottles, one containing a liquid precursor of vanadium, either $VOCl_3$ or VCl_4, and the other containing a liquid precursor of phosphorus, PCl_3. In this study, the molar concentration of each precursor in the *fuel stream* was set at 0.03%. The precursors react with oxygen which has diffused across the stagnation plane mostly in the form of radicals ($O\cdot$, $OH\cdot$, $H_2O\cdot$). Figure 2C shows the scattering intensity profile measured when 0.03% VCl_4 and 0.03% PCl_3 are added to the fuel stream of Flame 2. This scattering intensity profile can be thought as a map of where oxide formation and growth occur in the flame. It was obtained by sending an argon ion laser beam along the X direction of the burner, and detecting the light scattered at 90°, as a function of the Z elevation (10, 13). As one can see, the oxide forms at about $Z = -5.5$ mm, flows upward, and flows out at a particle stagnation plane (PSP) located at about $Z = -2.0$ mm. Particle stagnation planes are a characteristic of counterflow diffusion flames. Because of the sharp temperature gradients, particles experience thermophoretic forces (15, 16) pushing them toward the coolest region of the flame (i.e., the burner mouth). The particle stagnation plane is the location in the flame where these thermophoretic forces counterbalance the viscous forces due to the gas flow. At that location the particles are prevented from flowing further upward and they

TABLE 1
Flame Conditions and Gas Flow Rates

Flame #	Measured peak temperature (K)	Fuel stream (cc/min)		Oxidizer stream (cc/min)	
		H_2	Ar	O_2	Ar
1	2780	2263	1200	1818	167
2	2290	1239	2730	877	2760

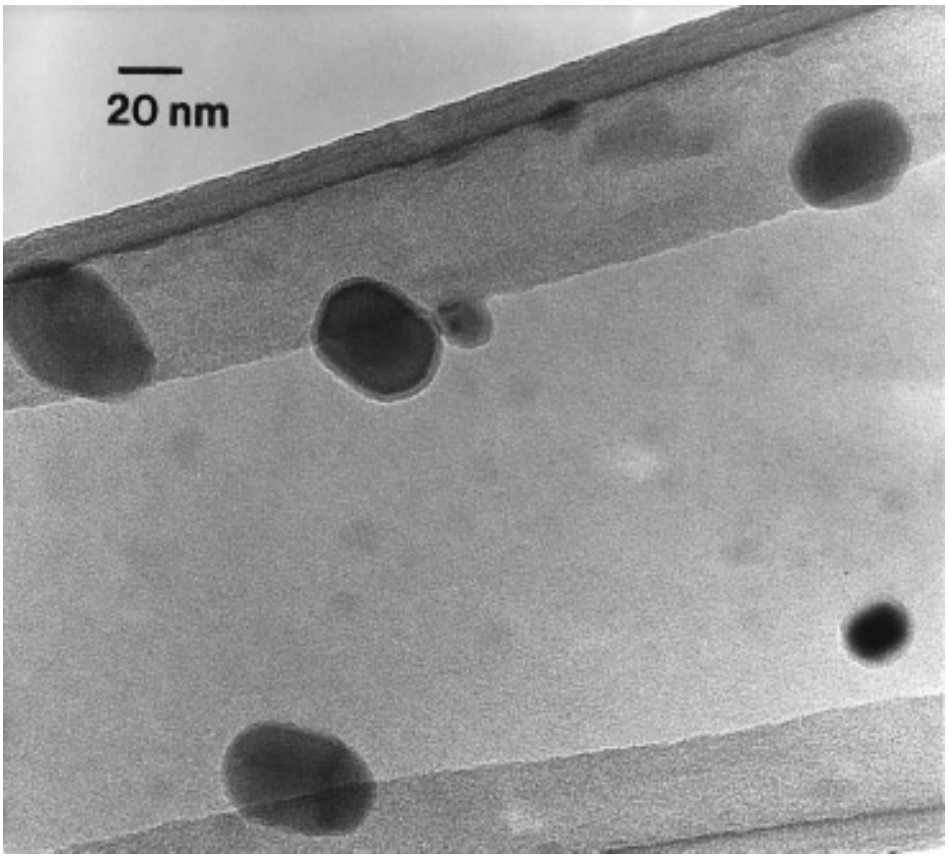

FIG. 3. Transmission electron micrograph of V–P–O particles collected in Flame 2.

therefore flow out of the burner. Figure 3 shows a transmission electron micrograph of particles collected *in* the flame itself at $Z = -2.2$ mm by very rapidly inserting and removing a transmission electron microscope grid (10, 13). Note that the average diameter of the particles collected on the grid is on the order of 30 nm. For a more complete description of vanadium–phosphorus oxide formation in the flames, the reader is referred to our previous publication (13).

Particles also were collected by allowing them to deposit onto stainless steel strips placed near the front and back sides of the burner (at about $Z = 0$ mm) (15, 17). The crystalline forms of the powders thus collected were determined using a Philips APD 3720 X-ray diffractometer (Cu$K\alpha$ radiation). The diffractometer was run over a 2θ angular range of 10° to 50°. Their FT-IR spectra also were measured at 2 cm^{-1} resolution using 32 scan averaging on a Mattson (Polaris) Fourier transform infrared spectrometer using the KBr disk technique (12, 13). The powders then were heated at about 700°C in flowing helium in a tube furnace for 5 hr. An oxygen-free atmosphere was ensured during heating by placing the powders, as a very thin layer, in the center of a titanium foil (Aldrich, 99.9%). Titanium is known to react very readily at these temperatures with even the slightest amounts of oxygen, to form TiO_2. When the titanium foil is not used, the same powders undergo oxidation upon heating, as shown previously (13).

RESULTS AND DISCUSSION

Vanadyl Pyrophosphate Precursors

Figures 4a and 4b are the X-ray diffraction patterns of powders collected on the stainless steel strips using Flame 1 and Flame 2, respectively. These XRD patterns were obtained on powders which were left in open atmosphere for about 5 days. As reported (13), these powders undergo rehydration during their exposure to the open atmosphere. Their XRD patterns prior to rehydration have broad diffraction lines. We believe it likely that both powders are nanocrystalline when they exit the flame and crystallize slowly upon contact with the water vapor present in the atmosphere. This recrystallization is caused by the very hygroscopic character of the flame-synthesized powders. Note that this hygroscopic property has been observed by others for a number of V–P–O phases (18, 19).

We previously attributed (13) the X-ray diffraction pattern of powders collected in Flame 1 to a mixture of

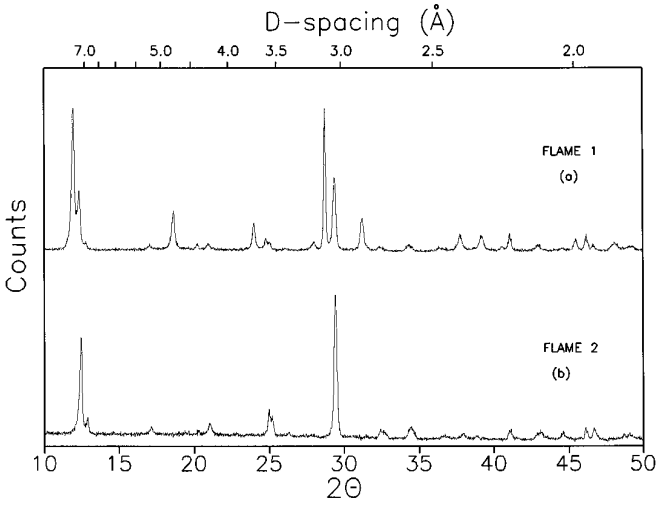

FIG. 4. X-ray diffraction patterns of powders collected in Flame 1 and Flame 2 after 5 days in open atmosphere.

TABLE 3
X-Ray Diffraction Lines of $(VOPO_4)_{1-x}$ $(VOHPO_4)_x \cdot 2.9H_2O$

This study		Amorós (20)	
d_{obs}	I/I_0	d_{obs}	I/I_0
7.05	71	7.07	100
6.84	11	6.85	38
5.15	5	5.15	8
4.21	8	4.31	11
3.53	13	3.54	30
		3.18	3
3.04	100	3.04	50
2.76	6	2.75	5
2.74	4		
2.61	8	2.61	5
1.945	18		
1.55			

$VOPO_4 \cdot 2H_2O$ (d-spacing = 7.41, 4.76, 3.70, 3.10, 1.96, 1.55 Å) and of an unknown $VOH_xPO_4 \cdot yH_2O$ (d-spacing = 7.18, 6.92, 3.59, 3.04, 2.29 Å). Comparison with diffraction patterns of existing V–P–O phases showed that the diffraction lines assigned to the unknown phase match those of a $(VOPO_4)_{1-x}(VOHPO_4)_x \cdot 2.6H_2O$ characterized by Amorós (20). The latter was obtained by precipitation upon adding a sulfite reducing agent (Na_2SO_3) to a H_3PO_4-$Ni(VO_3)_2$-H_2O solution (20). Table 2 compares the diffraction lines of our unknown phase to those of $(VOPO_4)_{1-x}$ $(VOHPO_4)_x \cdot 2.6H_2O$ synthesized by Amorós. In Flame 2, the XRD pattern of the powders collected was attributed by us (13) to an unknown $VOH_xPO_4 \cdot yH_2O$ phase. However, it does match the diffraction pattern of a $(VOPO_4)_{1-x}$ $(VOHPO_4)_x \cdot 2.9H_2O$ phase, also characterized by Amorós (20) (see Table 3), which he synthesized by refluxing a V_2O_5–H_3PO_4 mixture in a solution with excess NiI_2 as reducing agent.

TABLE 2
X-Ray Diffraction Lines of $(VOPO_4)_{1-x}(VOHPO_4)_x \cdot 2.6H_2O$

This study		Amorós (20)	
d_{obs}	I/I_0	d_{obs}	I/I_0
7.18	79	7.13	100
6.92	10	6.88	27
5.20	7		
4.24	8	4.2	5
3.59	16	3.57	17
3.04	100	3.03	89
2.77	5	2.75	5
2.61	8	2.60	5
2.29	21		

The powders collected in Flame 1 and Flame 2 are structurally similar. Their crystalline structure is characterized by a set of diffraction lines at d-spacings $\simeq$ 7.1, 6.9, 3.5, and 3.04 Å. This spacing appears to be characteristic of solid solutions of $VOPO_4 \cdot yH_2O$ phases ($y = 0, \ldots, 2$), the water being intercalated in the interlayer spacing. The high d-spacing lines, 7.18 or 7.05 Å are intermediate between the interlayer spacing (the (002) line) of $VOPO_4 \cdot 2H_2O$ and $VOPO_4 \cdot H_2O$, i.e., d = 7.4 and 6.3 Å, respectively. The ease with which both phases rehydrate upon contact with open atmosphere tends to confirm the layered structure. Note that the existence of stable solid solutions of a $(VOPO_4)_{1-x}(VOHPO_4)_x \cdot yH_2O$ type would explain the partial reduction ($V^{5+} \rightarrow V^{4+}$) of α_I-$VOPO_4$ upon hydration, observed previously by electron spin resonance (ESR) (19).

The report by Amorós is the only report we found in the literature which shows diffraction patterns in the V–P–O system similar to ours. However, in a recent investigation of the synthesis of V–P–O powders in a high-temperature aerosol reactor, Moser also reported the formation of an unknown powder (21). This powder was characterized by diffraction lines at d-spacings = 7.05, 3.54, and 3.05 Å. Note the similarity with the diffraction patterns of our $(VOPO_4)_{1-x}(VOHPO_4)_x \cdot yH_2O$ phases. Finally, another crystalline phase in the V–P–O system which has a diffraction pattern similar to that of $(VOPO_4)_{1-x}(VOHPO_4)_x \cdot yH_2O$ phases is the well known $VOH_{0.16}PO_4 \cdot 1.9H_2O$. This phase was characterized by Schneider (22) and observed by Harrouch Batis *et al.* after catalytic testing (4). $VOH_{0.16}$

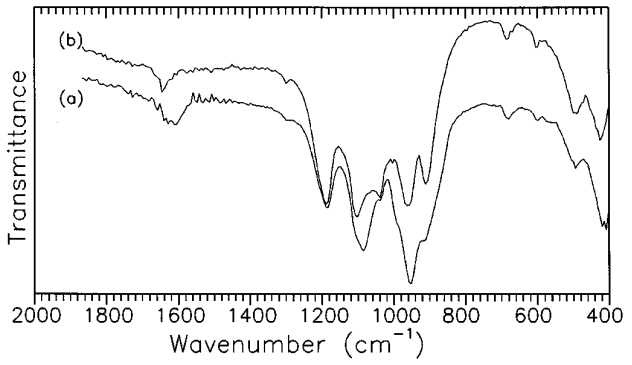

FIG. 5. FT-IR spectra of $(VOPO_4)_{1-x}(VOHPO_4)_x \cdot yH_2O$ phases before (a) and after (b) evacuation at 120°C for 18 hr.

$PO_4 \cdot 1.9H_2O$, whose chemical composition is consistent with that of a $(VOPO_4)_{1-x}(VOHPO_4)_x \cdot yH_2O$ structure, has reported diffraction pattern at d-spacing = 7.17, 6.96, 3.57 Å.

Spectrum (a) in Fig. 5 is the infrared spectrum of the powder collected in Flame 2. This spectrum is characteristic of $(VOPO_4)_{1-x}(VOHPO_4)_x \cdot yH_2O$ phases. Amorós' $(VOPO_4)_{1-x}(VOHPO_4)_x \cdot 2.9H_2O$ and $(VOPO_4)_{1-x}(VOHPO_4)_x \cdot 2.6H_2O$ phases, and also the powder we collected in Flame 1, show the same infrared lines (20). This spectrum is characterized by weak lines at 494, 599, 680 cm^{-1}, weak shoulders at 915 and 1039 cm^{-1}, and broad lines at 952, 1085, and 1183 cm^{-1}. Spectrum (b) in Fig. 5 shows the spectrum of the same powder after being in a vacuum at 120°C for 18 hr. Based on the IR band assignments for $VOHPO_4 \cdot yH_2O$ phases (5, 9), the weak bands at 494 and 599 cm^{-1} are attributed to δ(OPO). These lines are not affected by the vacuum treatment, which is consistent with this assignment. The weak shoulder at 915 cm^{-1} can be assigned to νP-(OH), which is in accord with its strengthening upon dehydration. Vanadyl (VO^{2+}) stretching vibrations lead to a sharp band in the 950–990 cm^{-1} region (23). The line at 952 cm^{-1} therefore can be assigned to ν(V=O). This vanadyl vibration is expected to be affected by the removal of water molecules. This can be observed in Fig. 5 as the line shifts towards high wavenumber after the vacuum treatment. The weak shoulder at 1039 cm^{-1} and the broad bands at 1085 and 1183 cm^{-1} are assigned to $\nu_{as}(PO)_3$.

Vanadyl Pyrophosphate Structures

Vanadyl pyrophosphate $(VO)_2P_2O_7$ is traditionally obtained by dehydration of $VOHPO_4 \cdot 0.5H_2O$ in nitrogen above 500°C (1, 2). Other $VOHPO_4 \cdot yH_2O$ phases, namely with y = 1, 2, 3, and 4, have been synthesized and characterized (7, 9). They too have been shown to transform into $(VO)_2P_2O_7$ when heated in inert atmospheres at temperatures between 100 and 500°C (9). Note that $VOHPO_4 \cdot yH_2O$ phases oxidize to (V^{5+}) $VOPO_4$ phases when heated in the presence of oxygen above 500°C (7, 9).

To investigate whether the powders produced in the burner were indeed precursors of vanadyl pyrophosphate, a similar heat treatment was applied. The powders produced in Flame 1 and 2 were first heated in a tube furnace in flowing helium to about 750°C (13). As reported previously, the powder produced in Flame 1 transformed into a γ-$VOPO_4$ phase under such heat treatment. An intermediate δ-$VOPO_4$ phase was observed upon heating at 390°C (13). The powder produced in Flame 2 transformed into β-$VOPO_4$ at 750°C, whereas an intermediate amorphous phase was obtained upon heating to 390°C. In both cases, the powders oxidized to V^{5+} phases, even though they were being heated in flowing helium, and the presence of V^{4+} (i.e., $(VO)_2P_2O_7$) was not detected. This unexpected oxidation may be due to the presence of oxygen in the helium stream. It represents an unusual behavior for $VOHPO_4 \cdot yH_2O$ phases, which tend to form V^{4+} phases when heated in inert atmospheres and may be due to the increased reactivity of our powders to oxygen because of their nanosize character or their dual $(VOPO_4)$/$(VOHPO_4)$ structure.

To confirm this hypothesis, new batches of powder were collected in both Flame 1 and Flame 2. These powders were then placed on titanium foils and heated in the tube furnace in flowing helium at 700°C. Figure 6 shows the X-ray diffraction patterns of the two powders thus formed. Both patterns match that of $(VO)_2P_2O_7$ published by others (7, 24). However, these diffraction patterns indicate structural differences between the two powders. For the powder from Flame 2 (the low temperature flame), a more

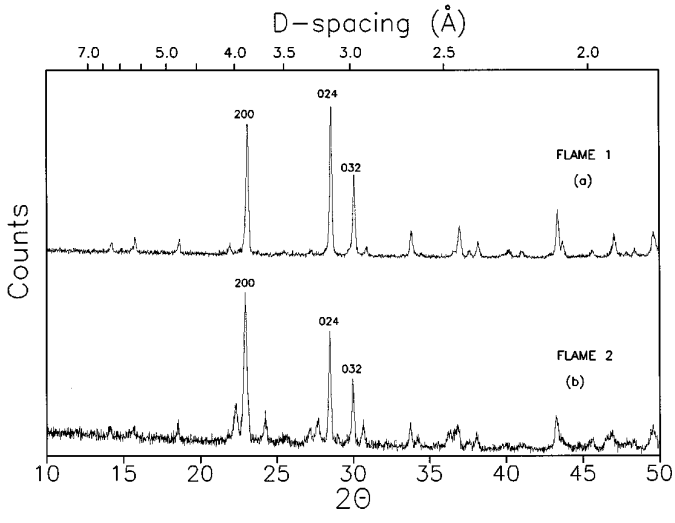

FIG. 6. X-ray diffraction pattern of $(VO)_2P_2O_7$ obtained by heating the powder collected in Flame 1 (a) and Flame 2 (b) on titanium foil at 700°C in flowing helium.

extensive development of the basal (100) $(VO)_2P_2O_7$ plane is indicated by the relative higher intensity of the corresponding (200) line (d-spacing = 3.86 Å). Note that the well-known platelet $(VO)_2P_2O_7$ structure (24, 25) typically exhibits a much higher relative intensity of the (200) line compared to that of the (024) and (032) lines. High relative intensity of the (200) line is generally associated with high catalytic activity and selectivity. Note that in spectrum (b), the three diffraction lines at d-spacing = 3.98, 3.67, and 3.22 Å do not match the diffraction pattern of $(VO)_2P_2O_7$, nor that of any other known V–P–O phase. However, they are relatively close to those of δ-$VOPO_4$ (d = 4.02, 3.68, 3.12, 3.21 Å). They also do not match the diffraction pattern of any titanium oxide phases, ruling out contamination from the titanium foil. The structural differences observed between the two powders are similar to the findings of Guilhaume *et al.* (3), who synthesized two vanadyl pyrophosphates by the traditional alcohol route using two different vanadium sources, one being a flame-synthesized V_2O_5. The highest activity they obtained was with a catalyst composed of a mixture of $(VO)_2P_2O_7$ with high (200) relative intensity and an additional α_{II}-$VOPO_4$ phase.

The ability of $(VO)_2P_2O_7$ to accommodate various disordered or polytypes structures was investigated recently by Thompson *et al.* (26). These authors used an idealized model of the $(VO)_2P_2O_7$ structure made up of vanadyl and pyrophosphate building blocks. The arrangements of these blocks lead to some 2^{16} possible variations of the structure, resulting in that many possible polytypes. Thompson *et al.* showed that one property of the $(VO)_2P_2O_7$ structure is that it can accommodate a large variety of interlayer vacancies. They also showed that irrespective of the block arrangements, the relative position of vanadium, phosphorus, and oxygen atoms is conserved, hence the X-ray diffraction pattern is identical for all the polytypes (although line intensities may vary with atomic order in the lattice). Gai and Kourtakis experimentally observed other disordered and/or polytypic transformations of $(VO)_2P_2O_7$ during catalytic testing (6). They observed extended defects along the [021] direction in butane-reduced $(VO)_2P_2O_7$. They suggested that gas–catalyst interaction generates anion vacancies (by loss of lattice oxygen), which diffuse into the crystal, causing the crystal to glide along the [021] direction to accommodate the misfit between the reduced surface layers. Under the proposed glide shear mechanism, the structure *and* the stoichiometry is preserved at the fault boundary. However, the resulting structure is a disordered structure of $(VO)_2P_2O_7$ differing only in local symmetry. The glide shear mechanism along the suggested direction is represented in Fig. 7. As one can see, it leads to the formation of corner sharing pairs of edge sharing vanadium octahedra and corner sharing pairs of corner shared phosphorus tetrahedra. These two investigations (6, 26) confirm the ability of $(VO)_2P_2O_7$ to exist under various disordered or polytypic structures. Note that the proposed disorders do *not* affect the bulk crystalline structure of $(VO)_2P_2O_7$. Hence, disordered structures have the same X-ray pattern of diffraction lines (although the relative intensity of the lines will vary). However, the symmetry of the structures and the local symmetry of the subunits in the structures, hence their IR spectrum, varies significantly with the type and the extent of disorder.

Spectra (a) and (b) in Fig. 8 show the FT-IR spectra of the powders whose XRD patterns are given in Fig. 6. Both spectra are consistent with that of $(VO)_2P_2O_7$. Furthermore, both spectra match that of β-$(VO)_2P_2O_7$ synthesized by Bordes *et al.* (25) by reduction of β-$VOPO_4$ in N_2 at 750°C. They (25) used the label β to distinguish between samples of $(VO)_2P_2O_7$ obtained by reduction of β-$VOPO_4$ (network structure) from those obtained by dehydration of $VOHPO_4 \cdot 0.5H_2O$ or by reduction of γ-$VOPO_4$ (platelet structure or γ-$(VO)_2P_2O_7$). In Fig. 8, spectrum (c) is the FT-IR spectrum of a platelet $(VO)_2P_2O_7$. Compared to

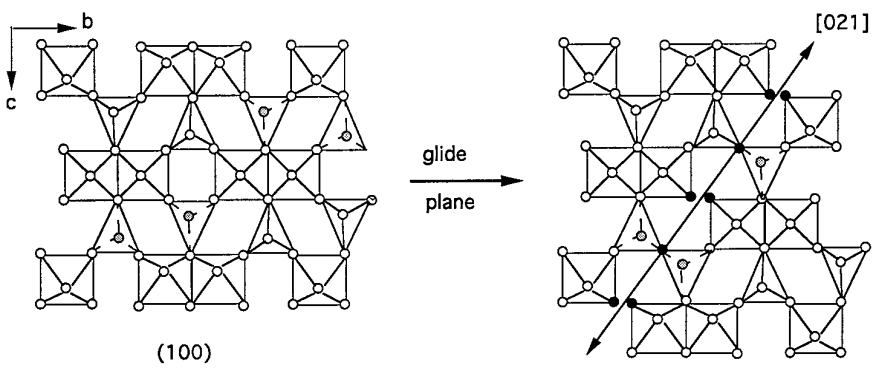

FIG. 7. (Left) Projection of a (100) layer of $(VO)_2P_2O_7$. (Right) Same projection showing the shear along the [021] direction as suggested by Gai and Kourtakis (6). Circles represent oxygen atoms (V and P atoms are not shown); grey circles: oxygen atoms behind the (100) plane; black circles: oxygen atoms to be connected between VO_6 and PO_4 units after accommodation of the lattice.

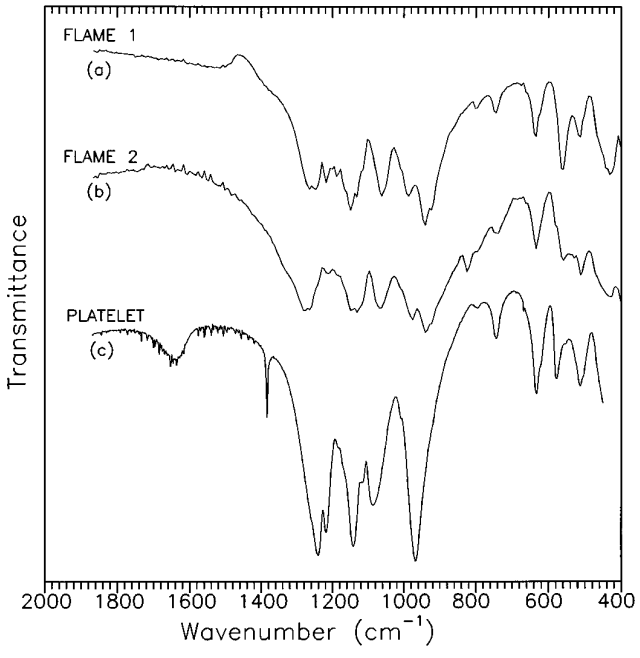

FIG. 8. Comparison of FT-IR spectra of $(VO)_2P_2O_7$ produced from powders collected using the burner when it was operating under (a) Flame 1 conditions or (b) Flame 2 conditions with (c) platelet $(VO)_2P_2O_7$.

spectrum (c), the main bands at 940, 1040, and 1260 cm^{-1} in spectra (a) and (b) exhibit significant splitting and shifting. This clearly indicates structural differences between the two vanadyl pyrophosphates produced using the burner and the platelet structure. Moreover, it also strongly suggest that "β" and "γ" are not two polymorphs of $(VO)_2P_2O_7$ as proposed by Bordes (25, 27) but polytypes with more or less disordered structures. Similarly, the two vanadyl pyrophosphates synthesized from powders collected in Flame 1 and 2 also are disordered or polytype structures of the platelet form of $(VO)_2P_2O_7$.

In the studies reported here, the precursors were added to the fuel stream. Thus, the particles nucleated and grew in an oxygen-poor region of the flame, making it likely that they would form oxygen-deficient structures. Moreover, nanostructured oxides are known to occur in nonstoichiometric structures (28). To accommodate the anion vacancies, during reduction in an oxygen-free atmosphere, glide shear mechanisms similar to those suggested by Gai and Kourtakis are likely to occur. The resulting structure is consistent with the differences observed between the IR spectrum of the vanadyl pyrophosphate generated using the burner (and also by Bordes (25)) and the platelet form of $(VO)_2P_2O_7$. The main differences are the 1250 and 1150 band, which are split and show shoulders. These bands were assigned to $\nu_{as}PO_3$ (5, 27). As one can see in Fig. 7, the glide shear mechanism along the [021] direction proposed by Gai and Kourtakis leads to the formation of pyrophosphate units sharing corners, locally similar to metaphosphate $(PO_3)_n$ groups. This would lead to additional $\nu_{as}PO_3$ vibrations, thus causing the observed splitting and/or shiftings of the bands. The same remark applies to the 920–980 band. This band, which is typical of V = O stretching modes (23), shows a significant amount of splitting for the two $(VO)_2P_2O_7$ powders produced using the burner, whereas it is very sharp at 960 cm^{-1} for the platelet form of $(VO)_2P_2O_7$ (see Fig. 8c). This splitting is consistent with the presence of two kinds of V = O environment, corner sharing and edge sharing vanadium octahedra, in the modified structure proposed by Gai and Kourtakis.

CONCLUSION

Vanadium–phosphorus mixed oxides powders were synthesized in a single step operation by a flame process. Two hydrated V–P–O phases were obtained by selecting two different flame conditions. The subsequent dehydration of these powders leads to the formation of γ-$VOPO_4$ and β-$VOPO_4$. Reduction of the same powders in an oxygen-free atmosphere leads to the formation of $(VO)_2P_2O_7$ in both cases. Structural differences between the two $(VO)_2P_2O_7$ were observed by X-ray diffractometry and infrared spectroscopy. These structural differences are consistent with the ability of the vanadyl pyrophosphate to accommodate a large variety of disordered structures. Moreover, they suggest that the two forms of $(VO)_2P_2O_7$ produced using the burner and the well-known β- and γ-$(VO)_2P_2O_7$ are different polytypes of the same vanadyl pyrophosphate phase.

The technique presented here is a novel route for the formation of the vanadium–phosphorus oxides. It greatly reduces the processing times necessary to produce such powders. Moreover, it allows one to select various particle morphology and crystalline structure by controlling the flame operating conditions. Finally, the average diameter of the particles produced by this technique is in the nanosize range. Powders composed of such powders show greatly enhanced surface area. They are expected to exhibit novel and enhanced catalytic properties.

ACKNOWLEDGMENTS

This work was supported by the Division of Materials Sciences, Office of Basic Energy Sciences, U.S. Department of Energy, via Grant DE-FG02-88ER45356.

REFERENCES

1. Bordes, E., *Catal. Today* **16,** 27 (1993).
2. Centi, E., Trifirò, F., Ebner, J., and Franchetti, V. M., *Chem. Rev.* **88,** 55 (1988).
3. Guilhaume, N., Rouillet, M., Pajonk, G., Grzybowska, B., and Volta, J. C., *Stud. Surf. Sci. Catal.* **72,** 255 (1992).

4. Harrouch Batis, N., Batis, H., Ghorbel, A., Vedrine, J. C., and Volta, J. C., *J. Catal.* **128,** 248 (1991).
5. Busca, G., Cavani, F., Centi, G., and Trifirò, F., *J. Catal.* **99,** 400 (1986).
6. Gai, P. L., and Kourtakis, K., *Science* **267,** 661 (1995).
7. Bordes, E., *Catal. Today* **1,** 499 (1987).
8. Bordes, E., *Catal. Today* **3,** 163 (1988).
9. Amorós, P., Ibáñez, R., Martinez-Tamayo, E., Beltrán-Porter, A., and Beltrán-Porter, D., *Mater. Res. Bull.* **24,** 1347 (1989).
10. Hung, C-H., and Katz, J. L., *J. Mater. Res.* **7,** 1861 (1992).
11. Hung, C-H., Miquel, P. F., and Katz, J. L., *J. Mater. Res.* **7,** 1870 (1992).
12. Miquel, P. F., Hung, C-H., and Katz, J. L., *J. Mater. Res.* **8,** 2404 (1993).
13. Miquel, P. F., and Katz, J. L., *J. Mater. Res.* **9,** 746 (1994).
14. Katz, J. L., and Hung, C. H., *Combust. Sci. Technol.* **82,** 169 (1992).
15. Miquel, P. F., Ph.D. Thesis, The Johns Hopkins University, Baltimore, MD, 1995.
16. Gomez, A., and Rosner, D. E., *Combust. Sci. Technol.* **89,** 335 (1993).
17. Miquel, P. F., and Katz, J. L., *Stud. Surf. Sci. Catal.* **91,** 207 (1995).
18. Ben Abdelouahab, F., Volta, J. C., and Olier, R., *J. Catal.* **148,** 334 (1994).
19. Ballutaud, D., Bordes, E., and Courtine, P., *Mater. Res. Bull.* **17,** 519 (1982).
20. Amorós, P., Master's Thesis, Universidad de Valencia, Valencia, Spain (1986).
21. Moser, W. R., *in* "Catalytic Selective Oxidation" (S. T. Oyama and J. W. Hightower, Eds.), ACS Symposium Series, p. 244. Am. Chem. Soc., Washington, DC, 1993.
22. Schneider, A., Thesis, Université de Bourdeaux, France 1987.
23. Selbin, J., *Chem. Rev.* **65,** 153 (1965).
24. Ben Abdelouahab, F., Olier, R., Guilhaume, N., Lefebvre, F., and Volta, J. C., *J. Catal.* **134,** 151 (1992).
25. Bordes, E., Courtine, P., and Johnson, J. W., *J. Solid State Chem.* **55,** 270 (1984).
26. Thompson, M. R., Hess, A. C., Nicholas, J. B., White, J. C., Anchell, J., and Ebner, J. R., *Stud. Surf. Sci. Catal.* **82,** 167 (1994).
27. Bordes, E., and Courtine, P., *J. Catal.* **57,** 236 (1979).
28. Parker, J. C., and Siegel, R. W., *J. Mater. Res.* **5,** 1246 (1990).